applied sciences

MDPI

Article

Proof of Concept of Crack Localization Using Negative Pressure Waves in Closed Tubes for Later Application in Effective SHM System for Additive Manufactured Components

Michaël F. Hinderdael *, Dieter de Baere and Patrick Guillaume

Department of Mechanical Engineering, Vrije Universiteit Brussel, Pleinlaan 2, 1050 Brussels, Belgium; dieter.de.baere@vub.ac.be (D.B.); patrick.guillaume@vub.ac.be (P.G.)

* Correspondence: mhinderd@vub.ac.be; Tel.: +32-2-629-28-07

Academic Editor: Nathalie Godin

Received: 17 November 2015; Accepted: 18 January 2016; Published: 25 January 2016

Abstract: Additive manufactured components have a different metallurgic structure and are more prone to fatigue cracks than conventionally produced metals. In earlier papers, an effective Structural Health Monitoring solution was presented to detect fatigue cracks in additive manufactured components. Small subsurface capillaries are embedded in the structure and pressurized (vacuum or overpressure). A crack that initiated at the component's surface will propagate towards the capillary and finally breach it. One capillary suffices to inspect a large area of the component, which makes it interesting to locate the crack on the basis of the pressure measurements. Negative pressure waves (NPW) arise from the abrupt encounter of high pressure fluid with low pressure fluid and can serve as a basis to locate the crack. A test set-up with a controllable leak valve was built to investigate the feasibility of using NPW to localize a leak in closed tubes with small lengths. Reflections are expected to occur at the ends of the tube, possibly limiting the localization accuracy. In this paper, the results of the tests on the test set-up are reported. It will be shown that the crack could be localized with high accuracy (millimeter accuracy) which proves the concept of crack localization on basis of NPW in a closed tube of small length.

Keywords: crack localization; negative pressure waves; structural health monitoring; additive manufacturing; fatigue cracks

1. Introduction

1.1. Additive Manufacturing

Additive manufacturing (AM), or 3D printing, is a new group of manufacturing technologies whereby physical objects are built by sequential addition of material on basis of a virtual 3D model.

These additive manufacturing techniques allow for completely different designs than the subtractive manufacturing techniques such as milling, grinding, drilling, *etc.*, which require that a tool can reach the spot that has to be shaped (which is not always possible). With 3D printing, the cost is merely related to the amount of printed material, not to the complexity of the design. As the tendency exists to produce components at the lowest possible cost, there exists a stimulus to reduce the weight of 3D printed components, which is a clear benefit in several sectors such as aeronautics. Three-dimensional printed components also possess the property of embedding smart technologies during the printing process, generating overall smart solutions.

As additive manufactured components are constructed layer by layer, their metallurgic structure is different from conventionally produced materials. Fatigue and crack propagation properties

of additive manufactured materials are not very well known yet [1], because a lack of process understanding and a lack of *in situ* process monitoring and control, especially in metal AM systems, currently results in unknown porosity levels and distributions [2]. Multiple sources report a reduced fatigue lifetime. In the work of Chan *et al.* [3], fatigue lifetime of titanium Ti6Al-4V alloys fabricated by means of additive manufacturing were compared to conventionally produced Ti6Al-4V alloys (rolled or cast). Conventionally rolled Ti6Al-4V alloys showed approximately twice the fatigue lifetime of the best additive manufactured Ti6Al-4V alloys. Gong *et al.* [4] stated that as-built surfaces of selective laser melted (SLM) Ti-6Al-4V samples become crack initiation sites, resulting in a reduced fatigue lifetime when the stress level exceeds 500 MPa. Similar results were also recorded in the paper of Strantza *et al.* [5], where the SLM Ti6Al-4V samples indicated a stress level at failure under fatigue loading of 590 MPa and 570 MPa.

Despite the numerous benefits, the reduced fatigue behavior is currently jeopardizing the introduction of additive manufactured primary components in industries where safety and product availability are very important. Inspection intervals must then be shortened, increasing inspection costs and product unavailability, which inevitably induce large economic losses. Including an effective structural health monitoring system that monitors the fatigue behavior of 3D printed components can largely eliminate this major drawback.

1.2. Effective Structural Health Monitoring System

Structural health monitoring (SHM) is the integration of sensing and possibly also actuation devices to allow the damaging conditions of a structure to be recorded, analyzed, localized and predicted in a way that non-destructive testing becomes an integral part of the structure [6].

Many structural health monitoring principles have been developed in laboratory conditions but suffered problems when introduced in real applications. Grease, environmental changes, electrical noise, vibrations and many other external influences have shown to have a severe impact on the performance of these structural health monitoring systems. Despite the clear benefits of an SHM system, but due to this lack of robustness, only a few systems have made the transition from the laboratory to a real application [7,8]. A successful structural health monitoring system must be robust in the first place: very low false alarm rates, high detectability of the cracks and insensitive to external influences.

Bearing this in mind, a new effective structural health monitoring philosophy (eSHM) was recently developed [7]. Small subsurface capillaries are embedded in the structure by means of additive manufacturing techniques, close to the region where fatigue cracks are expected to grow. The capillaries are then pressurized (vacuum or overpressure) and the capillary pressure is monitored continuously during the operation of the component. A crack, that initiated at the surface of the component, propagates through the material until it finally breaches the capillary. The resulting leak changes the internal capillary pressure. The presence of a fatigue crack is then derived from the moment that the capillary pressure bypasses a certain pre-set limit. In Figure 1, a possible application of the new effective SHM system is depicted. The embedded capillaries are indicated in red.

The capillaries of the eSHM system must be embedded in the regions where fatigue cracks are expected to grow. In order not to reduce the strength of the component, one must take into account the presence of the capillaries during the design phase. It was concluded in the paper of Strantza *et al.* [9] that—for the considered structure in the paper—the presence of the capillary did not influence the fatigue life negatively, although the cracks initiated from the capillary when positioned close to the specimen edge. Another paper of Strantza *et al.* [10] reported on four point bending test results of test samples with a different layout of the embedded capillaries. It was concluded that the capillary had no crucial influence on the fatigue initiation location for the test specimen and test conditions under investigation. Future studies are being focused on robustness improvements of the eSHM to delay crack initiation at the capillary location.

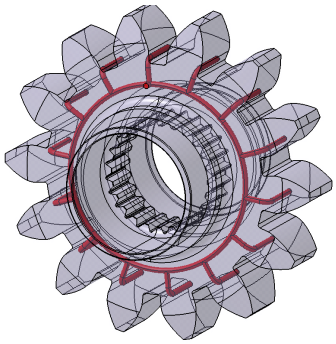

Figure 1. Embedded capillaries (in red) of the effective Structural Health Monitoring System (eSHM) [7].

Embedding the capillary in a way that it connects all locations prone to fatigue allows monitoring the critical areas without the need for multiple sensing devices. In the example of the cogwheel of Figure 1, only one pressure measurement is required to inspect all teeth. This largely facilitates the installation, data storage and post-processing of the data of the eSHM system. After detection of a fatigue crack, further analysis has to be performed on the critical area. It is therefore interesting to know, on basis of the pressure measurement, where the cracked region is located (e.g., which tooth suffers from a crack).

1.3. Negative Pressure Waves

Negative pressure waves (NPW) serve as a basis for the inspection of pipelines. As explained in the paper of Wan *et al.* [11], when a leak happens along the pipeline, the fluid density of the leak point declines immediately due to the fluid medium losses and the pressure drops. Then the pressure wave source spreads out from the leak point to both ends of the pipeline. The analysis of the time-of-arrival of these wave fronts at known locations at both sides of the leak then allows for locating the leak with high accuracy. In the paper of Silva *et al.* [12], NPW are analyzed to locate leaks in pipelines under operation (with flow). The paper reports that the leak in the pipeline could be located with an accuracy comparable to the theoretical uncertainty related to the finite sampling rate that was used.

In this paper, the authors will analyze if NPW can also be used to locate a leak in a closed volume (without flow), as will be the case in the embedded capillaries of the eSHM system. The static pressure inside the volume will continuously change as a consequence of the leak flow, which is not the case in the well known pipeline applications. First, simulations are discussed to understand the nature and amplitude of the negative pressure waves. Secondly, measurements on a test set-up are discussed and the crack localization capability on the basis of negative pressure waves in a closed volume is analyzed.

By installing a pressure sensor at each side of the closed tube, one can measure the difference in time-of-arrival of the two waves. The time needed for the NPW to travel to the two sensors is easily deduced from Figure 2. For the latter part of this paper, the sensor with name 'S1' will always be referring to the sensor which is closest to the leak (it receives the signal first), while sensor 'S2' will be the sensor located far from the leak (receiving the signal later).

$$\text{Sensor S1} \quad t_1 = \frac{x_1}{c} \tag{1}$$

$$\text{Sensor S2} \quad t_2 = \frac{L - x_1}{c} \tag{2}$$

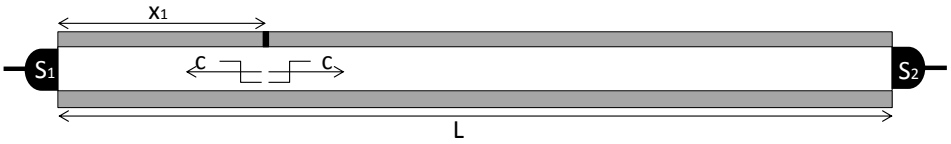

Figure 2. The difference in time-of-arrival of the negative pressure waves at the two pressure sensors mounted at both ends of the tube allows for locating the crack.

Because t_1 and t_2 are only known relatively, only combination of Equations (1) and (2) leads to a localization formula:

$$x_1 = \frac{L - c(t_2 - t_1)}{2}. \tag{3}$$

The theoretical uncertainty on the crack location (Δx) is related to the sampling rate ($f_s = \frac{1}{\Delta T_s}$) of the data acquisition unit through

$$\Delta x = \frac{c\Delta T_s}{2} = \frac{c}{2f_s}. \tag{4}$$

Because of the high sonic speeds (for air at room temperature: $c = \sqrt{kRT} = 343\frac{m}{s}$), it will be required to use a high sampling rate to reduce the uncertainty on the estimated location and to deduce the localization feasibility. A sampling rate of 204.8 kHz, for instance, results in a theoretical uncertainty on the location of the leak of 0.84 mm.

For the ease of practical implementation, the capillaries are represented by 3/4" tubes (diameter of 16.9mm) and with a length of 462 mm. The circular leak had a diameter of 1mm. The initial pressure level is set at approximately 20 kPa (absolute) while the outside environment is at ambient conditions (101.3 kPa). The temperatures are expected to be all in equilibrium at room temperature (293.15 K). The performed simulations and measurements discussed in the following parts of the paper will always be referring to this test set-up.

We can estimate the amplitude of the NPW on basis of the formula derived by Rocha [13] (and summarized in the paper of Loth *et al.* [14]):

$$\Delta P_{cap} = 0.3 P_{atm} \left(\frac{D_{leak}}{D_{tube}} \right)^2. \tag{5}$$

Given the diameters of the tube ($D_{tube} = 16.9mm$) and leak ($D_{leak} = 1mm$), and the ambient conditions around the tube ($P_{atm} = 101300$Pa), we expect the amplitude of the NPW to be:

$$\Delta P_{cap} = 0.3 \times 101300 \text{ Pa} \times \left(\frac{1 \text{ mm}}{16.9 \text{ mm}} \right)^2 = 106.5 \text{ Pa}. \tag{6}$$

It must be noted here that one calls the acoustic waves "NPW" as they were first analyzed and used in pipeline applications. These pipelines are mostly put under overpressure to distribute liquids over large distances. A leak lowers the internal pressure, which is the reason why the occurring waves are referred to as "NPW". In a vacuum application, which we will be using in the eSHM system, the amplitude of the wave will be positive (increasing pressure), so that the name "Positive Pressure Waves" is more opportune. However, this name has never been used in the literature before. We will therefore stick to the name NPW, although the sign of the pressure change depends on the pressurization case.

2. Simulations

Simulations in "COMSOL Multiphysics" were performed in order to understand the nature of the NPW in more detail. As we are interested in the development and propagation of the NPW, a time-dependent analysis was chosen. Because of a small leak, laminar flow was assumed. The tube with the crack, as described in Section 1.3, is represented by a large cylinder (the tube) connected to another smaller cylinder (the crack). Both cylinders contain air that is assumed to be initially at rest. The air is at an absolute pressure of 20 kPa (vacuum). When the crack is opened, air will enter through the small cylinder (the crack). Therefore, a pressure condition (equal to the ambient pressure) is set to this inlet surface. The no slip condition is applied to all other walls. In order to interpret the development and propagation of the NPW, the plots only contain the pressure information in the range of 20,000–20,200 Pa (as is expected from Equation (6)).

Figure 3 shows the pressure results of the computational fluid dynamics analysis (CFD) obtained in a section in the longitudinal direction of the tube. The abrupt opening of the crack results in a discontinuity of the pressure at the crack location. Assuming that the capillary pressure is below the ambient pressure, the low pressure on the inside of the capillary meets the relative higher pressure of the atmosphere. That discontinuity results in a local increase of density and pressure at the crack location. The pressure wave further propagates through the crack and expands as a spherical wave front in the tube. Once in the tube, the spherical wave front forms two plane waves that travel in opposite directions at the speed of sound (c) through the capillary.

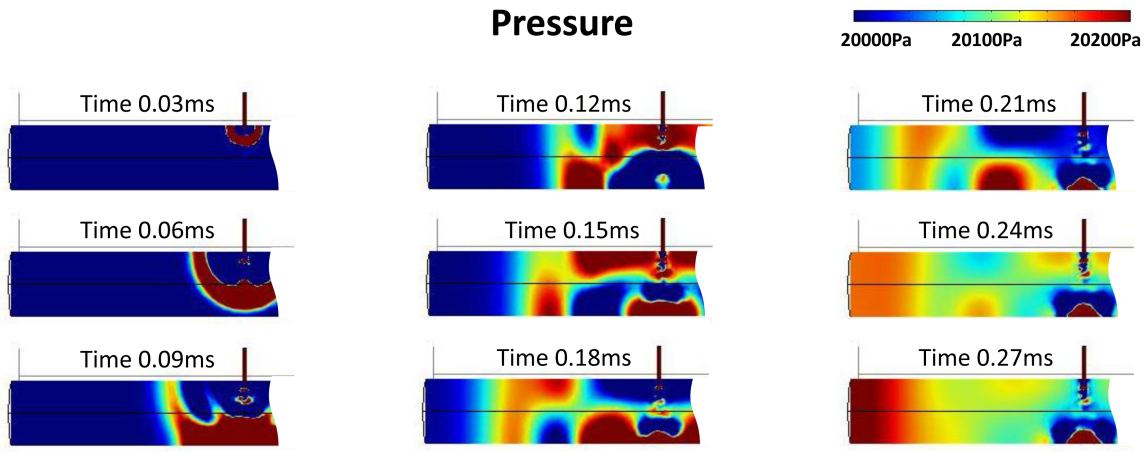

Figure 3. Computational fluid dynamics analysis of negative pressure waves.

The last time step in Figure 3 clearly indicates that when the NPW arrive at the end of the tube (acoustically seen as a hard wall), the amplitude of the NPW doubles because the incident wave is in phase with the reflected wave. The reflected wave then travels back to the other side of the tube where it will be detected by the other sensor. The amplitude of the arriving NPW is 100 Pa (doubled at the wall).

3. Experimental Set-Up

A test set-up was built to investigate the crack localization capability on the basis of the NPW. For the ease of practical implementation, the capillaries are represented by 3/4" tubes (internal diameter of 16.9mm) and with a length of 462mm. Along the longitudinal direction of the tube, multiple connections are foreseen to simulate different leak positions and to pull vacuum. A detailed drawing of the tube can be seen in Figure 4 and a graphical presentation of the test-setup is given in Figure 5. The circular leak had a diameter of 1 mm. The initial pressure level is set at approximately 20 kPa (absolute) while the outside environment is at ambient conditions (101.3 kPa). The temperatures are expected to be all in equilibrium at room temperature (293.15 K).

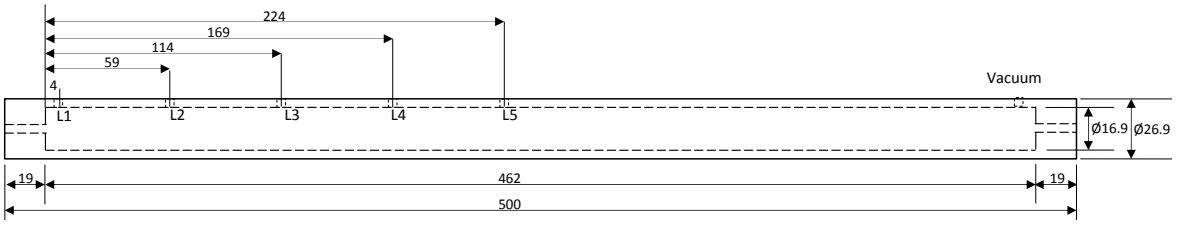

Figure 4. Drawing of the 3/4" tube of the test set-up (dimensions in mm).

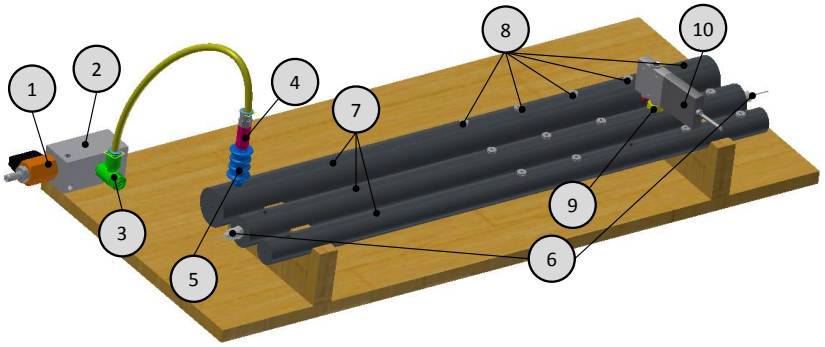

①	Shut-off valve
②	Venturi
③	Flow controller
④	Check valve
⑤	Shut-off valve
⑥	Pressure sensors
⑦	Tubes
⑧	Leak positions
⑨	Leak size
⑩	Solenoid valve

Figure 5. Graphical presentation of the test set-up.

Along the length of the tube, multiple holes were foreseen to simulate different leak positions (called L1 to L5 from left to right in Figure 4). During a test, all but one were closed while the remaining hole was connected to a solenoid on–off valve to simulate the opening of the crack with a known diameter of 1mm. The last hole, on the right along the length direction of the tube, was used to pressurize at the required initial pressure level before the measurement.

The tube was closed at both ends and each side was equipped with a pressure sensor (Endevco MEGGIT 8540-200). The sensor was selected such that it could measure static pressure changes with a sufficiently high sensitivity (noise level about 10–20Pa, much below the expected amplitude of the NPW (see Equation (6))). The sensors were connected to a LMS Scadas III mobile data acquisition system with a maximum sampling rate of 204.8 kHz. Such a high sampling rate is needed to lower the theoretical uncertainty on the location of the leak to a value of 0.84 mm (see Equation (4)).

4. Results and Discussion

In the following sections, the measurements on the test set-up will be analyzed to derive the crack localization feasibility on basis of the NPW. First, the measurement at leak location L2 will be explained in detail and the location of the leak will be estimated on basis of the pressure measurements. ($x_1 = 59$ mm as defined in Figure 2). Secondly, the measurements at different leak locations will be compared and the localization results on these measurements will be summarized.

4.1. Detailed Analysis of Leak Position L2

Figure 6 presents the pressure measurements for leak location L2 obtained from sensors S1 (full line) and S2 (dashed line). The plot is focused at the moment of time-of-arrival of the NPW at the two sensors and is zeroed at the initial pressure level. Vertical line 0 corresponds to the theoretical moment of opening the leak. Vertical lines 1 and 2 then correspond to the moment of time-of-arrival at sensors S1 and S2 of which the times are given below the figure.

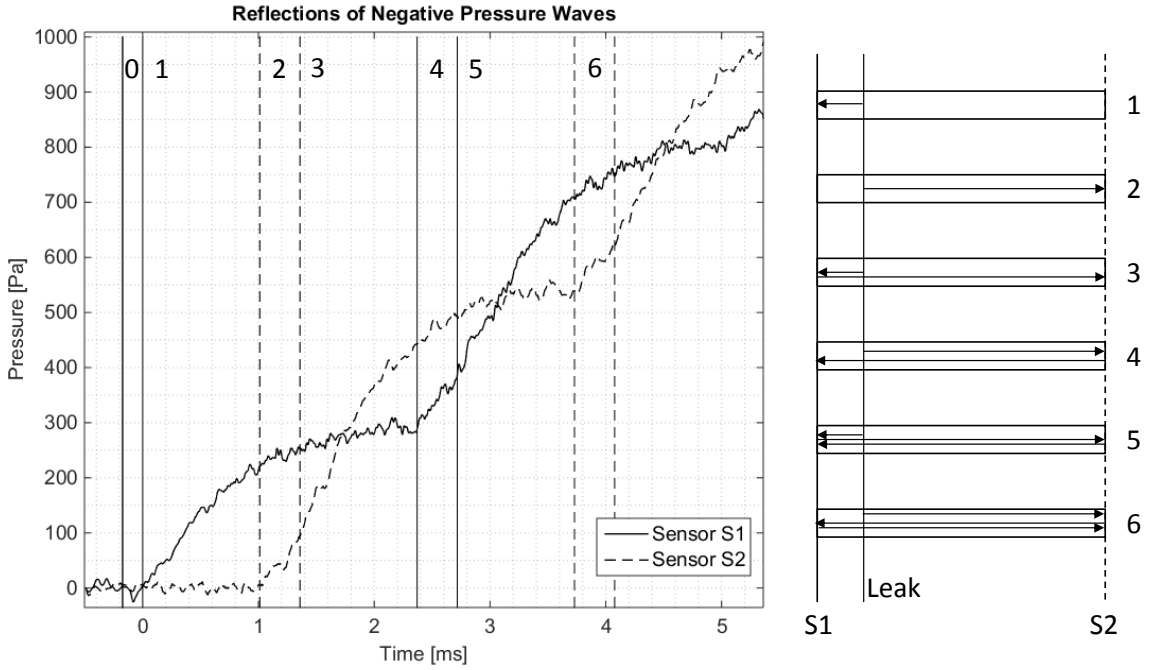

Sensor S1	TOA = 0.00 ms
Sensor S2	TOA = 1.03 ms

Figure 6. Time-of-arrival of the (reflections of) negative pressure waves.

It must be noted that Figure 6 shows the presence of pressure steps, rather than a continuous increase of the pressure. This is due to the reflections of the NPW at the hard walls of the tube (where the sensors are located). Vertical line 4, for instance, corresponds to the moment of arrival at sensor S1 of the NPW that first went to the side of sensor S2 (and was measured there at the moment corresponding to vertical line 2) and then reflected back to the side of sensor S1.

The static pressure change can thus be seen as a succession of exponential pressure steps. The measurement of sensor S1 clearly shows a first exponential pressure rise between vertical lines 1 and 4. A second, less clear exponential pressure step starts at vertical line 4 and ends at vertical line 5 where a third exponential pressure step starts. That exponential behavior is the reason why the breakpoint at vertical line 4 is more clear than at vertical line 5: the more the exponential has flattened, the more the slope of the two successive exponentials differ and the clearer the breakpoint becomes. The recognition of a breakpoint in the pressure steps also allows location of the leak, just by using one pressure sensor [15].

To evaluate the amplitude of the NPW and to compare with the theoretical prediction (Equation (6)), one must must take into account that the sensor measures twice the amplitude of the NPW because of the hard wall at which the wave reflects and the pressure adds up (see section 2). Together with this effect, it is important to note that, due to the contribution of a direct wave and the contribution of a reflected wave that arrives a bit later, multiple NPW might contribute to the pressure rise we are investigating. The pressure rise on sensor S2 between vertical line 2 and 6 flattens out when approaching vertical line 6. We can thus assume that the amplitude of that pressure step can be approximated to the value at vertical line 6, i.e. 530 Pa. Breakpoint 3, however, corresponds to the moment that a second, reflected, wave arrives at the location of sensor S2. The pressure between vertical lines 2 and 6 thus corresponds to the addition of two NPW with amplitude 530 Pa/2/2 = 132.5 Pa. This is in rather good correspondence with the theoretical prediction 106Pa (Equation (6)) and the simulations 100 Pa (see Section 2).

Given the moments of time-of-arrival of the direct waves below the figure, it is possible to estimate the crack location on basis of Equation (3).

$$x_1 = \frac{0.462 - 343 \times 0.00103}{2} \text{ m} = 54.4 \pm 0.84 \text{ mm}. \quad (7)$$

This estimate has to be compared to the real location of the leak, which is 59 mm. We can conclude that the estimation of the leak position is rather good but still larger than the theoretical minimum (related to the finite sampling rate (204.8 kHz)). The remaining error is due to noise present on the measurements, which makes it difficult to select the exact moment of arrival of the NPW.

4.1.1. Sensitivity of Leak Localization Technique

It must be highlighted that the measurements are sensitive to the selection of the point of time-of-arrival which is not always easy to select due to noise. Therefore, a sensitivity analysis of the leak localization technique on basis of the NPW was performed. We therefore assume that the moment of time-of-arrival on Sensor S1 is correct, and we show the theoretical interval of detection of the time-of-arrival on Sensor S2 to have a localization of the leak with an error lower than ± 1 cm. The following figure, Figure 7, presents the same measurement as Figure 6 but is more focused on the moments of time-of-arrival at the sensors. The region corresponding to an inaccuracy of ± 1 cm on the localization of the leak was added around the theoretical time-of-arrival at sensor S2.

It must be clear from this measurement that the presence of noise negatively affects the localization accuracy. It is feasible to locate the leak with relative high accuracy, but we must allow an uncertainty in the approximation of a centimeter, which is an order of magnitude larger than the theoretical limit related to the finite sampling rate. Improvement of the test set-up to reduce the noise (e.g. by use of lower range pressure sensors with a higher sensitivity and resolution, *etc.*) or better processing techniques can solve this issue and increase the localization accuracy. In the following section, one example of a better processing technique is given.

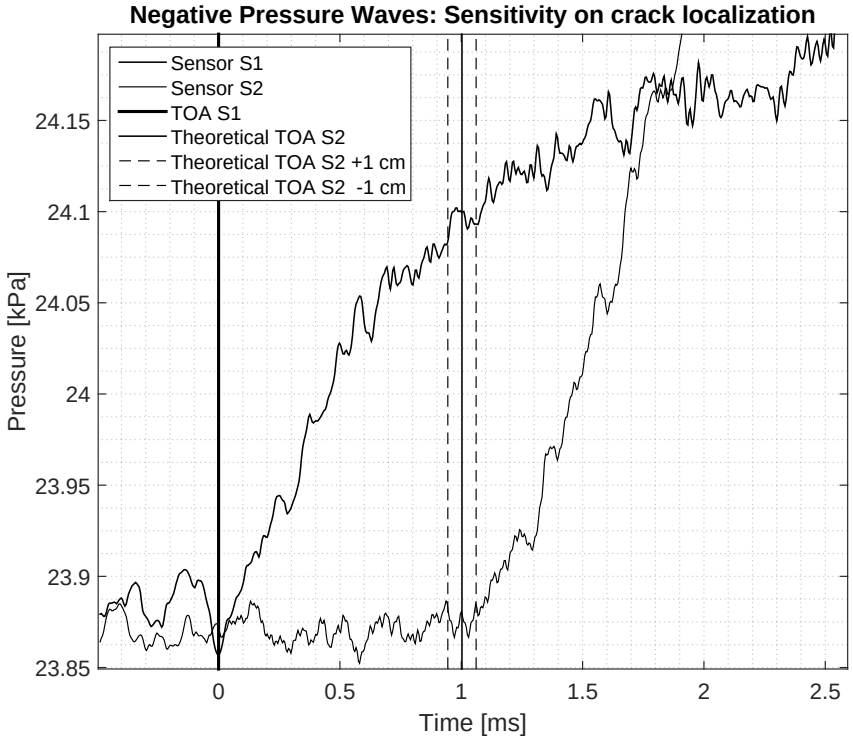

Figure 7. Sensitivity analysis for time-of-arrival point selection for crack localization.

4.1.2. Improvement of the Leak Localization Technique Due to Least Squares Method

Up to now, the difference in time-of-arrival of the NPW was defined as the difference in time between the points where the pressure starts increasing. That principle is very prone to the effects of noise as the selection of these points can be different on basis of the noise that is present on the signal. We therefore aim for a different method to estimate the difference in time-of-arrival of the NPW. The principle is based on a least squared method on the first rising part of the NPW. The signal of sensor S2 is shifted in time and compared with the measurement of sensor S1. The optimum shift of the signal is found when the least squares analysis reports the smallest error between the two signals. The plot in the top right corner of Figure 8 indicates the part of the signal of Figure 6 that will be used for the analysis. The bottom right corner shows that the optimum was found when the signal of sensor S2 was shifted 207 datapoints to the left. The resulting match is plotted on the left of the same figure.

Based on this analysis, we can now estimate the location of the leak. We therefore again use Equation (3):

$$x_1 = \frac{0.462 - 343 \times \frac{207}{204800}}{2} \text{ m} = 57.7 \pm 0.84 \text{ mm}. \quad (8)$$

This location should again be compared to the exact distance, 59mm. This method clearly reduces the effect of noise on the localization of the leak. The error now falls within the theoretical uncertainty related to the finite sampling rate. Improving the localization accuracy (e.g., by using better processing techniques) enables the reduction of the sampling rate of the data acquisition while keeping the error on the localization constant, which is an important cost reduction when considering a later application in the eSHM system. Much research has been performed in the past to improve the leak localization accuracy for pipeline applications such as that presented in the papers of Ostapkowicz [16] and Srirangarajan *et al.* [17].

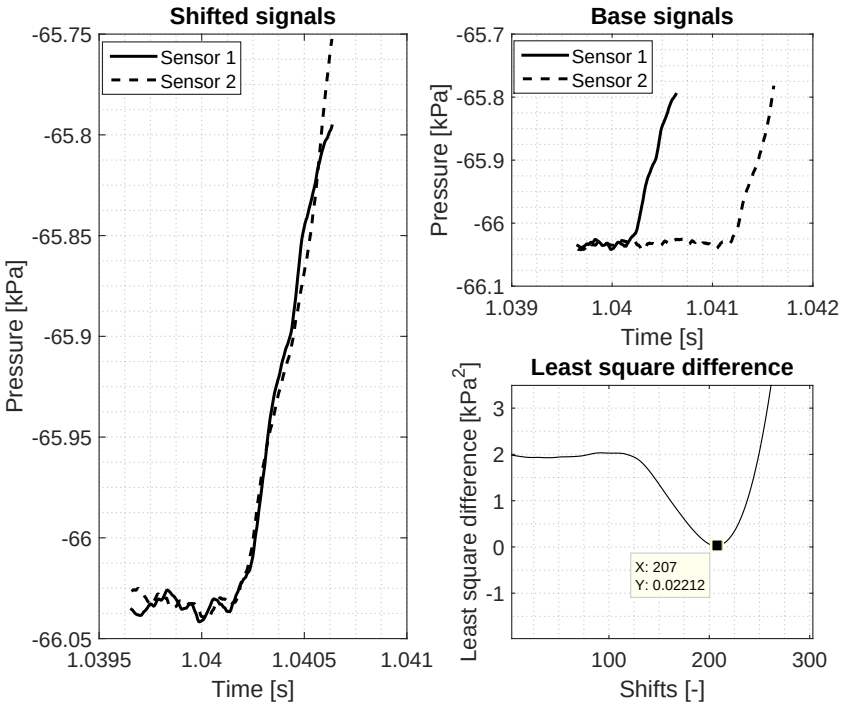

Figure 8. Least square analysis on time-of-arrival of negative pressure waves originating from leak position L2.

4.2. Different Leak Positions

As stated in Section 3 and indicated in Figure 4, multiple leak locations (L1–L5) were foreseen on the tube. As to evaluate the leak localization feasibility, it must be possible to distinguish the different leak locations (L1 to L5) from the obtained difference in time-of-arrival of the NPW. Figure 9 contains five different measurements for the five different leak locations (L1–L5). The thick vertical line corresponds for all five measurements to the moment of time-of-arrival of the NPW at sensor S1. The figure only shows the data measured at sensor S2. The difference in time-of-arrival between sensor S1 (reference) and S2 (increasing pressure) is compared for the different leak locations.

The more the leak is positioned near the middle of the tube (L5), the smaller the difference in time-of-arrival at the sensor locations because the NPW travelled approximately equal times to both ends of the tube. The NPW that originated from L1, the most extreme leak position, clearly arrived with a large time delay at sensor S2.

The theoretical moments of time-of-arrival corresponding to the different leak locations are highlighted through the thin vertical lines. It is clear from the analysis of Figure 9 that the different leak locations can be separated on basis of the interpretation of the NPW.

The least squares method allows to estimate the leak position with high accuracy. Table 1 summarizes the localization estimations and errors of all five measurements (L1–L5).

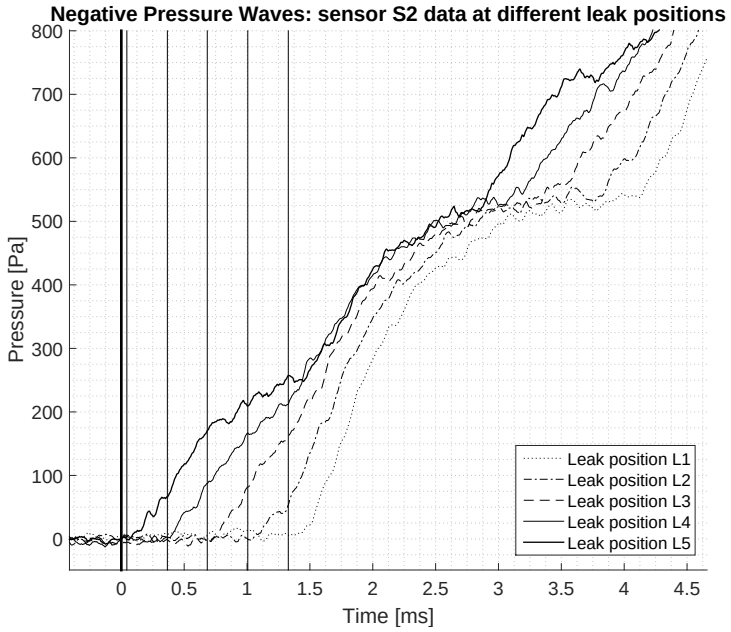

Figure 9. Comparison of the difference in time-of-arrival for different leak positions.

Table 1. Localization feasibility on basis of time-of-arrival of the negative pressure waves using the least squares analysis. (L_{tube} = 462 mm).

Nº	Location $x_{1,real}$ (mm)	Localization Estimate $x_{1,est}$ (mm)	Error $\frac{x_{1real}-x_{1,est}}{L_{tube}}$ %
*L*1	4	7.4	0.736
*L*2	59	57.6	0.303
*L*3	114	109.6	0.952
*L*4	169	167.4	0.346
*L*5	224	222.6	0.303
Average			0.528

The average error on the location of the leak is found to be

$$\text{Error} = \frac{0.528}{100} \times 0.462 \text{ m} = 2.4 \text{ mm}. \quad (9)$$

This error is not much more than the theoretical limit due to the finite sampling rate, which allows us to conclude that the NPW analysis can be used to locate the crack with high accuracy.

5. Conclusions

Recently, a new effective structural health monitoring methodology was presented whereby capillaries are embedded in a 3D printed structure in order to monitor the presence of fatigue cracks. As multiple critical regions of the components can be inspected by means of just one capillary, it is of interest to investigate the crack localization possibilities on the basis of the pressure signals measured in the capillaries. Therefore, a feasibility study was performed on a test set-up with a controllable leak valve using closed tubes that imitate the capillaries of the presented system. The static pressure change in the closed tube is found to be a succession of pressure steps, corresponding to the arrivals of (the reflections of) NPW. As with pipelines, the difference in time-of-arrival of NPW is investigated in order to locate the leak in closed tubes. It was found that the difference in time-of-arrival allows to locate the leak, but that the selection of the exact moment of time-of-arrival is prone to noise fluctuations which significantly reduced the accuracy of the localization. Better processing techniques, such as a leasts squares analysis, allowed for the reduction of the localization uncertainty to approximately the theoretical limit related to the finite sampling rate (millimeters). We can therefore conclude that we validated the proof-of-concept of crack localization on the basis of NPW in closed tubes.

Acknowledgments: The research work was financed by the Agency for Innovation by Science and Technology in Flanders (IWT) and the Strategic Basic Research project SBO 110070 eSHM with AM.

Author Contributions: The authors contributed equally to the presented work through discussions, improvements and analysis of the obtained measurements.

Conflicts of Interest: The authors declare no conflict of interest.

References

1. Wycisk, E.; Solbach, A.; Siddique, S.; Herzog, D.; Walther, F.; Emmelmann, C. Effects of Defects in Laser Additive Manufactured Ti-6Al-4V on Fatigue Properties. *Phys. Proced.* **2014**, *45*, 371–378.
2. Slotwinski, J.A.; Garboczi, E.J.; Hebenstreit, K.M. Porosity Measurements and Analysis for Metal Additive Manufacturing Process Control. *J. Res. Natl. Inst. Stand. Technol.* **2014**, *119*, 494–528.
3. Chan, K.S.; Koike, M.; Mason, R.L.; Okabe, T. Fatigue Life of Titanium Alloys Fabricated by Additive Layer Manufacturing Techniques for Dental Implants. *Metall. Mater. Trans. A* **2013**, *44*, 1010–1022.
4. Gong, H.; Rafi, K.; Starr, T.; Stucker, B. Effect of defects on fatigue tests of as-built Ti-6Al-4V parts fabricated by selective laser melting. In Proceedings of the 23rd Annual International Solid Freeform Fabrication Symposium, Austin, Texas, USA, 6–8 August 2012, 499–506.
5. Strantza, M.; de Baere, D.; Rombouts, M.; Clijsters, S.; Vandendael, I.; Terryn, H.; Guillaume, P.; Van Hemelrijck, D. 3D Printing for Intelligent Metallic Structures. In Proceedings of the EWSHM 7th European Workshop on Structural Health Monitoring, Nantes, France, 8–11 July 2014.
6. Boller, C.; Meyendorf, N. State-of-the-art in Structural Health Monitoring of Aerospace Structures. In Proceedings of the International Symposium on NDT in Aerospace, Fürth, Bavaria, Germany, 3–5 December 2008.
7. De Baere, D.; Strantza, M.; Hinderdael, M.; Devesse, W.; Guillaume, P. Effective Structural Health Monitoring with Additive Manufacturing. In Proceedings of the EWSHM 7th European Workshop on Structural Health Monitoring, Nantes, France, 8–11 July 2014.
8. Farrar, C.R.; Worden, K. An introduction to Structural Health Monitoring. *Philos. Trans. R. Soc. A: Math. Phys. Eng. Sci.* **2007** *365*, 303–315.

9. Strantza, M.; Vafadari, R.; de Baere, D.; Rombouts, M.; Vandendael, I.; Terryn, H.; Hinderdael, M.; Rezaei, A.; van Paepegem, W.; Guillaume, P.; *et al*. Evaluation of Different Topologies of Integrated Capillaries in Effective Structural Health Monitoring System Produced by 3D Printing, In Proceedings of the 10th International Workshop on Structural Health Monitoring, Stanford University, Stanford, CA, USA, 1–3 September 2015.
10. Strantza, M.; de Baere, D.; Rombouts, M.; Maes, G.; Guillaume, P.; van Hemelrijck, D. Feasibility study on integrated structural health monitoring system produced by metal three-dimensional printing. *Struct. Health Monit.* **2015**, doi:10.1177/1475921715604389.
11. Wan, J.; Yu, Y.; Wu, Y.; Feng, R.; Yu, N. Hierarchical Leak Detection and Localization Method in Natural Gas Pipeline Monitoring Sensor Networks *Sensors* **2012**, *12*, 189–214.
12. Silva, R.A.; Buiatti, C.M.; Cruz, S.L.; Pereira, J.A.F.R. Pressure wave behaviour and leak detection in pipelines. *Comput. Chem. Eng.* **1996**, *20*, S491–S496.
13. Rocha, M.S. Acoustic Monitoring of Pipeline Leaks. In Proceedings of the Instrument Society of America (ISA) Symposium, Calgary, Alberta, Canada, 3–5 April 1989.
14. Loth, J.L.; Morris, G.J.; Palmer, G.M.; Guiler, R.; Mehra, D. Technology Assessment of On-Line Acoustic Monitoring for Leaks/Infringements in Underground Natural Gas Transmission Lines. In *Task 3 for DOE Contract DE-FC26-02NT413424*; Daniel Driscoll: NETL Morgantown, WV, USA, 2003.
15. Misiunas, D.; Vitkovsky, J.; Olsson, G.; Simpson, A.; Lambert, M. Pipeline Break Detection Using Pressure Transient Monitoring. *J. Water Resour. Plan. Manag.* **2005**, *131*, 316–325.
16. Ostapkowicz, P. Leakage detection from liquid transmission pipelines using improved pressure wave technique. *Eksploat. Niezawodn.* **2014**, *16*, 9–16.
17. Srirangarajan, S.; Allen, M.; Preis, A.; Iqbal, M.; Lim, H.B.; Whittle, A.J. Wavelet-Based Burst Event Detection and Localization in Water Distribution Systems. *J. Signal Process. Syst.* **2012**, *72*, 1–16.